Chapter 2. Physics of proton interactions in matter

Jan Unkelbach

Abstract

The Bragg peak is the most remarkable feature of the proton depth dose curve, which drives the interest in using proton beams for radiotherapy. This chapter discusses the interactions of protons in matter that are the most important in the context of proton therapy. The main goal is to explain the dose distribution of a proton beam, starting from the fundamental physical interactions. This forms the basis for dose calculation algorithms and the design of beam-modifying devices such as scatterers and range shifters. Protons in the energy range relevant for radiotherapy (up to around 300 MeV) interact in tissue mainly through three types of interactions. 1) Coulomb scattering with atomic electrons, 2) Coulomb scattering with atomic nuclei, and 3) Nuclear interactions. Coulomb scattering with electrons results in gradual loss of energy of a proton while traversing a medium. Consequently, coulomb scattering with electrons mainly determines the depth dose curve of a proton beam. The chapter provides an approximate classical deviation of the Bethe-Bloch equation and the effect of range straggling. Coulomb scattering with nuclei leads to small angular deflections of protons and thus determines the width and the broadening of the beam with depth. The chapter starts with the Rutherford cross section and derives the Rossi formula for multiple coulomb scattering. Nuclear interactions, also referred to as hard scatters, are relatively rare events. As a rough rule of thumb, approximately 1% of protons undergo a nuclear interaction per centimeter of distance travelled in water. Nuclear interactions make a relatively small, but not negligible, correction to the depth dose curve. In addition, nuclear interactions may result in large scattering angles and lead to dose contributions outside the primary proton beam, which is referred to as the nuclear halo. By the end of the chapter, the main physical interactions of protons in matter are discussed, and a basic Monte Carlo algorithm to calculate the characteristic dose distribution of a Gaussian proton beam is introduced.

Table of Content

2.1. Introduction

This chapter discusses the interactions of protons in matter that are the most important in the context of proton therapy. The main goal is to explain the dose distribution of a proton beam, starting from the fundamental physical interactions. This forms the basis for dose calculation algorithms, which are discussed in more detail in later chapters of this book (chapter 17). Besides dose calculation, understanding the physical interactions of protons is also relevant for other aspects of proton therapy, e.g. the design of beam-modifying devices such as scatterers and range shifters (chapters 4 and 5).

Protons in the energy range relevant for radiotherapy (up to around 300 MeV) interact in tissue mainly through three types of interactions:

1. Coulomb scattering with atomic electrons (section 2.2)
2. Coulomb scattering with atomic nuclei (section 2.3)
3. Nuclear interactions with nuclei (section 2.4)

Coulomb scattering with electrons results in a gradual loss of energy of a proton while traversing through a medium. Consequently, coulomb scattering with electrons mainly determines the depth dose curve of a proton beam. Coulomb scattering with nuclei leads to small angular deflections of protons and thus determines the width and the broadening of the beam with depth. Nuclear interactions, also referred to as hard scatters, are relatively rare events. As a rough rule of thumb, approximately 1% of protons undergo a nuclear interaction per centimeter of distance traveled in water. Nuclear interactions make a relatively small, but not negligible, correction to the depth dose curve. In addition, nuclear interactions may result in large scattering angles and lead to dose contributions outside the primary proton beam, which is referred to as the *nuclear halo*.

Nowadays, Intensity-modulated proton therapy (IMPT) is delivered using narrow, Gaussian-shaped proton beams of varying energy that are magnetically scanned across the target volume (chapter 4). At the end of this chapter (section 2.5), we will have described the physical interactions of protons in matter that allow us to calculate the characteristic dose distribution of a Gaussian proton beam as shown in figure 2.11.

While many aspects of proton therapy have evolved and improved over time, e.g. through the further development of delivery technology or treatment planning algorithms as described in later chapters, the basic laws of physics relevant that govern the physical interactions of protons in matter are time-invariant. The theory of coulomb interactions of protons with electrons and nuclei have been developed approximately 100 years ago and has not changed since. The classic textbooks "Classical electrodynamics" by Jackson [1] or "The atomic nucleus" by Evans [2] are valuable references.

2.1.1. A simple model of the proton depth dose curve

The Bragg peak is the most remarkable feature of the proton depth dose curve, which drives the interest in using proton beams for radiotherapy of deep-seated tumors. In this section

and the following section 2.2, we aim to understand how the depth dose curve of a proton beam comes about, considering the underlying physical interactions. To that end we initially consider a broad proton beam where all protons travel along the z-direction in 3D space, and we assume the particle fluence to be constant in the xy-plane perpendicular to the beam direction. The protons hit the surface of a homogeneous medium at $z = 0$ with an initial proton energy E_0. The lateral dose distribution of a proton beam in the xy-plane will afterwards be discussed in sections 2.3-2.5.

Dose is defined as energy deposition per unit mass. To develop a simple model of the depth dose curve, let us consider the energy that is transported by primary protons through a unit area in the x-y plane perpendicular to depth direction z. This is called the energy fluence $\psi(z)$, which has the units of energy per unit area[1]. The energy fluence depends on the energy $E(z)$ that these protons have at that depth, and the particle fluence $\phi(z)$, i.e. the number of primary protons at depth z per unit area:

$$\psi(z) = \phi(z)E(z) \tag{2.1}$$

If we assume for now that all protons always travel along the z -direction, and that all energy that it is transferred to secondary particles is absorbed locally, then the dose $D(z)$ deposited at depth z is given by the derivative of the energy fluence

$$D(z) \approx -\frac{1}{\rho}\frac{\psi(z)}{dz} = -\frac{1}{\rho}\left[\frac{E(z)}{dz}\phi(z) + \frac{\phi(z)}{dz}E(z)\right] \tag{2.2}$$

The first term on the right-hand side of equation (2.2) describes the dose deposition due to gradual energy loss of primary protons due to electromagnetic interactions with atomic electrons (which does not change the particle fluence $\phi(z)$). The second term describes energy deposition due to the absorption of primary protons in nuclear interactions. In equation (2.2), we divide by the mass density ρ of the medium (with units of mass per volume) because of the definition of dose as energy deposition per unit mass rather than unit volume.

Equation (2.2) is only an approximation of the depth dose curve of a proton beam because it assumes that all energy transferred to secondary particles by primary protons is deposited locally. This is approximately true for coulomb interactions with electrons. The energy transfer to most electrons is small in the sense that the electron travels only a short distance from the interaction point. However, the energy that is transferred to secondary particles in nuclear interactions is in part carried away from the interaction point and deposited elsewhere. Equation (2.2) is nevertheless an instructive first approximation of the proton depth dose curve, because $D(z)$ is dominated by the first term $E(z)/dz$ whereas the second term can be considered as a correction term. The derivation of $E(z)/dz$ is thus the most important part in understanding the depth dose curve and will be discussed in section 2.2.

[1] In general, the energy fluence is a vector field $\vec{\psi}(x, y, z)$. For now, we assume, however, that all protons travel along the z-axis such that we only have to consider the z-component ψ_z. A generalization to the 3-dimensional case will be considered in section 2.5.3.

2.2. Energy loss

In this section, we discuss the electromagnetic interaction of protons with electrons, i.e. coulomb scatting. Coulomb scattering with electrons results in an energy transfer from the incident proton to the electron. By myriad collisions with electrons, the incident proton gradually loses energy while traversing matter and eventually stops in the medium. This interaction is the most important for explaining the depth dose curve of a proton beam and the existence of the Bragg peak. The energy loss of protons due to coulomb scattering with electrons is very accurately described by the *Bethe-Bloch equation*. Subsection 2.2.1 starts with a description of the Bethe-Bloch equation and the derivation of the proton depth dose curve in continuous slowing down approximation (CSDA), which would represent the proton depth dose curve in a hypothetical world without nuclear interactions. Afterwards, the relation of proton energy and range is discussed (section 2.2.2). Subsequently, we provide an approximate derivation of the Bethe-Bloch equation from the classical theory of coulomb scattering (section 2.2.3) and derive the effect of range straggling resulting from statistical fluctuations in the number of collisions (section 2.2.4).

2.2.1. The Bethe-Bloch equation

We consider a proton that traverses a homogeneous medium. Energy loss of protons due to coulomb scattering with electrons is described by the Bethe-Bloch equation. For the energy range relevant to proton therapy (in the order of approximately 3 to 300 MeV), the Bethe-Bloch equation is typically stated as

$$\frac{dE}{dz} = -\left(\frac{1}{4\pi\varepsilon_0}\right)^2 \frac{4\pi e^4 N_e}{m_e c^2 \beta^2}\left[\ln\left(\frac{2m_e c^2\beta^2}{I(1-\beta^2)}\right) - \beta^2\right] \tag{2.3}$$

where dE/dz denotes change in energy dE of a proton when traveling a small distance dz through the material. c is the speed of light and $\beta = v/c$ is the velocity of the proton, which determines its energy. The material that the proton beam penetrates is characterized by the electron density N_e and the mean ionization potential I. The mean ionization potential is the mean energy that is needed to ionize the atom/molecule, i.e. the mean energy that needs to be transferred to an electron bound in an atom/molecule to remove the electron from the shell. The remaining parameters are fundamental constants. ε_0 is the vacuum permittivity, m_e is the mass of the electron, and e is the charge of the electron and the proton. The term

$$\frac{2m_e c^2\beta^2}{(1-\beta^2)} = \Delta E_{\max} \tag{2.4}$$

in the logarithm is the maximum energy that can be transferred to a single electron in a head-on collision under conservation of energy and momentum. The velocity β of a relativistic proton relates to its kinetic energy via the relativistic energy momentum relation

$$E = \frac{m_p c^2}{\sqrt{1-\beta^2}} - m_p c^2 \tag{2.5}$$

By replacing β^2 in equation (2.3) with the proton energy, we can think of the Bethe-Bloch equation as an ordinary differential equation for the proton energy E as a function of depth z. By solving the differential equation numerically, we obtain the residual proton energy $E(z)$ along its path, and the derivative dE/dz yields the energy loss.

The electron density N_e is defined as the number of electrons per unit volume. It relates to the mass density ρ via the relation

$$N_e = \rho \frac{N_A}{M_u} \frac{Z}{A} \tag{2.6}$$

where N_A is the Avogadro constant (the number of atoms/molecules per mole), M_u is the molar mass (1g per mole), Z is the number of electrons per atom/molecule, and A is the number of nuclei per atom/molecule. Since Z/A is in the order of 0.5 and does not vary largely between different materials, the electron density is mainly proportional to the mass density of the medium. The right-hand side of the Bethe-Bloch equation is also referred to as the *stopping power* S of a material as it alludes to the ability of a medium to "stop the protons". As we see from equations (2.3) and (2.6), the stopping power and the energy loss of a proton per unit path length are proportional to the mass density of the material. The ionization potential I introduces an additional material dependence of the stopping power. However, this additional dependence is relatively weak compared to the impact of the mass density[2].

In radiotherapy, water is used as the reference medium because most soft tissues in the body mainly consist of water. For water, chemically H_2O, the ratio of electrons and nuclei is $Z/A = 10/18$. The literature value for the mean ionization potential of water is 75 eV, and the density is 1 g/cm^3. By numerically solving the Bethe-Bloch equation, assuming water as the medium and an initial proton energy E_o of 100 MeV, we obtain the result shown in figure 2.1, where the proton energy is measured in MeV and distance is measured in mm.

Starting with the initial energy E_o at $z = 0$, protons gradually lose energy until at a distance R_o all energy is transferred to electrons and the proton stops (blue line). R_o is called the range of the proton beam, which depends on the initial energy E_o. The red line in figure 2.1 shows the derivative dE/dz, that is, how the proton depth dose curve would look like in a hypothetical world without nuclear interactions and without the effect of range straggling discussed in section 2.2.4. This is also referred to as the *continuous slowing down approximation* (CSDA). In this case, dE/dz has a singularity at R_o. The energy loss per unit path length increases with decreasing residual energy, and therefore increases with depth. This aspect is further explained in section 2.2.3 where an approximate derivation of the Bethe-Bloch equation is provided.

There are several correction terms to the Bethe-Bloch equation as stated in equation (2.3), which are relevant for very low or very high energies but can be neglected in the context of proton therapy. Good modern accounts with many references can be found in introductions

[2] The ionization potential usually cannot be calculated accurately from first principles. Therefore, it is often considered an adjustable parameter of the theory, which can be fine-tuned to establish agreement with experimental data.

to the range-energy tables of Janni[34] and ICRU (International Commission on Radiation Units and Measurements) Report 49[5].

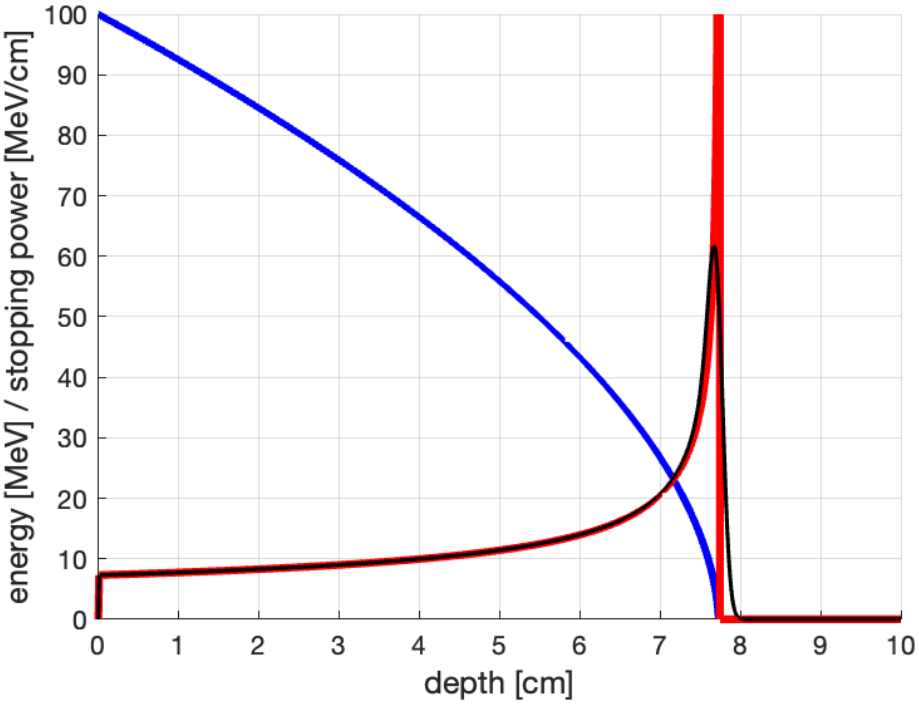

Figure 2.1: Energy E (blue line) and energy loss dE/dz (red line) as a function of depth in water, obtained by numerically solving the Bethe-Bloch equation for protons with an initial energy of 100 MeV. The black line is obtained by convolving dE/dz with a Gaussian distribution with a standard deviation of 0.82 mm to account for range straggling.

2.2.2. The energy-range relation

By solving the Bethe-Bloch equation, we can determine the range R_o of a proton beam depending on the initial energy E_0. This is called the energy-range relation. Here is a short energy-range table for water, where the range is measured in cm and the proton energy in MeV:

energy E_0 [MeV]	10	30	50	100	200	300
range R_o [cm H_2O]	0.125	0.896	2.2	7.793	26.0	51.87

[3] J. F. Janni, Calculations of energy loss, range, pathlength, straggling, multiple scattering, and the probability of inelastic nuclear collisions for 0.1 to 1000 MeV protons, Air Force Weapons Laboratory Technical Report No. AFWL-TR-65-150 (1966).

[4] J. F. Janni, Proton range-energy tables, 1KeV–10 GeV, Atomic Data and Nuclear Data Tables 27 parts 1 (compounds) and 2 (elements) (Academic Press, 1982).

[5] M.J. Berger, M. Inokuti, H.H. Andersen, H. Bichsel, D. Powers, S.M. Seltzer, D. Thwaites, D.E. Watt, H. Paul and R.M. Sternheimer, Stopping powers and ranges for protons and alpha particles, ICRU Report 49 (1993).

The range increases more than linearly with the initial energy of the protons. The range as a function of energy can be described very accurately by a power law

$$R_0 = \alpha E_0^p \tag{2.7}$$

Fitting this equation to the range in water, we obtain the fit parameters $\alpha = 0.0022$ and $p = 1.77$. Interestingly, equation (2.7) gives rise to an analytical representation of dE/dz, which can then be extended to an analytical description of the proton depth dose curve as described by Bortfeld [3]. To that end, let $E(z)$ be the residual proton energy at depth z. Then, the residual range $R(z)$ of the protons at depth z is given by

$$R(z) = R_0 - z = \alpha E(z)^p \tag{2.8}$$

because equation (2.7) must hold at any depth z. The residual energy $E(z)$ is thus

$$E(z) = \alpha^{-1/p}(R_0 - z)^{1/p} \tag{2.9}$$

which yields

$$\frac{dE(z')}{dz'}(z) = \frac{1}{p\alpha^{-1/p}}(R_0 - z)^{(1/p)-1} \tag{2.10}$$

2.2.3. An approximate classical derivation of the Bethe-Bloch equation

A complete derivation of the Bethe-Bloch equation (2.3) requires a relativistic and quantum mechanical theory of coulomb scatting from atomic electrons, which is outside the scope of this chapter. However, the main terms and dependencies in the Bethe-Bloch equation can be derived from a simple classical model of the interaction.

The proton and the electron interact via the Lorentz force

$$\vec{F} = \frac{1}{4\pi\varepsilon_0}\frac{e^2}{r^2}\frac{\vec{r}}{|\vec{r}|} \tag{2.11}$$

where $\vec{r}$ is the vector that describes the position of the proton relative to the electron. The force between the two particles gives rise to the equation of motion

$$\vec{F} = \frac{\partial}{\partial t}\vec{p}(t) \tag{2.12}$$

which relates the force to the change in momentum, i.e. the acceleration of the particles. The equation of motion can be solved analytically in this case. Since the mass of the proton is three orders of magnitude larger than the mass of the electron, we can make several simplifying assumptions to proceed. First, the proton will travel approximately along a straight line, and we can neglect the minimal change in the proton's direction during the scattering event. Second, let us assume that the electron is initially at rest at position $\vec{r} = 0$. We may assume that the electron moves little during the scattering event, such that the

distance and the force between proton and electron can be calculated as if the electron remained at $\vec{r} = 0$. This leads to the simplified model of the process that is illustrated in figure 2.2.

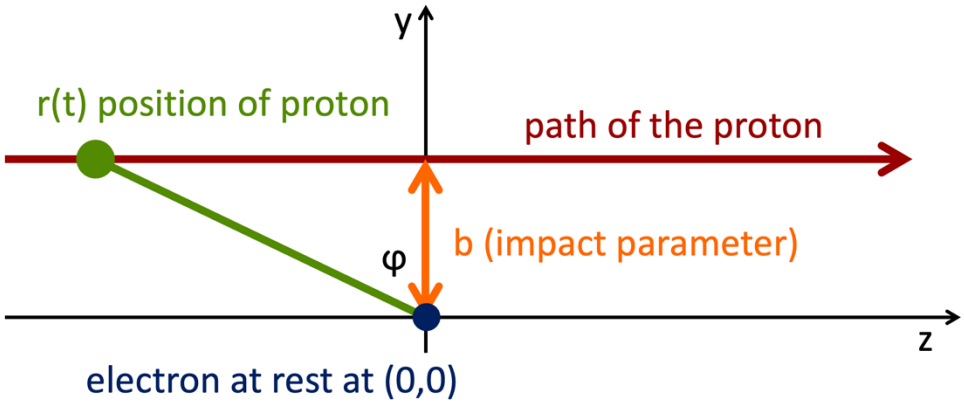

Figure 2.2: Classical model of coulomb scattering of a proton from an electron.

We consider a proton that is incident along the z-axis with velocity v and passes an electron located at $\vec{r} = 0$ at distance b, where b is called the *impact parameter*. From the Lorentz force we can calculate the total momentum transfer to the electron during the process. The momentum transfer in a direction perpendicular to the proton's direction of travel, y, is given by integrating the y-component of the Lorentz force:

$$\Delta p_y = \int_{-\infty}^{+\infty} F_y(t)\, dt = \int_{-\infty}^{+\infty} \frac{1}{4\pi\varepsilon_0} \frac{e^2}{r(t)^2} \cos\varphi(t) dt \qquad (2.13)$$

The total momentum transfer in the direction of travel, z, can be evaluated analogously by integration of the z -component of the Lorentz force. However, due to the symmetry of the problem, the z -component of the Lorentz force at position z will be equal to the force at position $-z$ but with opposite sign. Consequently, the total momentum transfer in z -direction will be zero and we only need to consider the direction perpendicular to the proton's path.

We can transform the integration over time t in (2.13) into an integration over position z using $z = vt$ which yields

$$dt \to \frac{1}{v} dz \qquad (2.14)$$

when we assume the velocity of the proton to be approximately constant. By further using that the distance r can be expressed via the impact parameter b and the angle φ through $b = r\cos\varphi$ we obtain

$$\Delta p_y = \int_{-\infty}^{+\infty} \frac{1}{4\pi\varepsilon_0}\frac{e^2}{b^2}\frac{1}{v}\cos^3\varphi(z)\,dz \tag{2.15}$$

Using $z = r\sin\varphi$ we can transform the integration over the path z into an integration over the angle φ. Through $dz \to \frac{b}{\cos^2\varphi}\,d\varphi$ we obtain

$$\Delta p_y = \int_{-\pi/2}^{+\pi/2} \frac{1}{4\pi\varepsilon_0}\frac{e^2}{bv}\cos\varphi\,d\varphi = \frac{1}{4\pi\varepsilon_0}\frac{2e^2}{bv} \tag{2.16}$$

The momentum transfer Δp_y corresponds to an energy transfer Q given by

$$Q = \frac{\Delta p_y^2}{2m_e} = \left(\frac{1}{4\pi\varepsilon_0}\right)^2 \frac{2e^4}{m_e v^2}\frac{1}{b^2} \tag{2.17}$$

This expression describes the energy transfer to a single electron at distance b from the proton track. It highlights the important property that 1) the energy transfer is larger if the electron is closer to the proton track, and 2) the energy transfer is larger if the incident proton is slower.

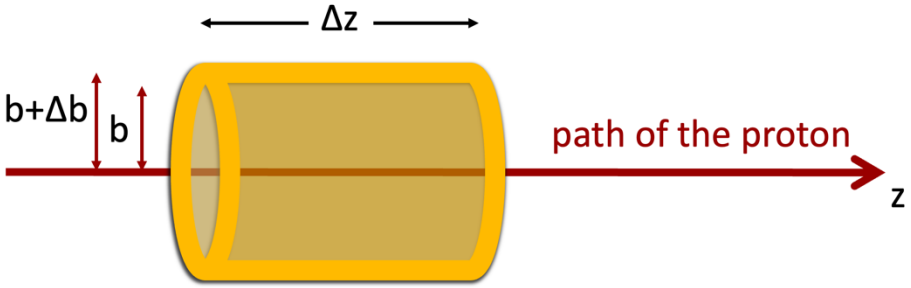

Figure 2.3: Illustration of energy loss of a proton over a distance Δz by integrating over the energy transfers to electrons in a cylinder around the proton track.

Next, we want to obtain the total energy loss of a proton ΔE while the proton travels a small distance Δz through a medium. For that we must integrate the energy transfers to all electrons that are located around the proton track. To that end, we assume that the medium has a homogeneous electron density N_e which describes the number of electrons per unit volume. Let us first consider the energy loss due to all electrons that are located in a cylindrical shell of length Δz, thickness Δb and radius b around the proton track, which is illustrated in figure 2.3. The volume of this cylindrical shell is $2\pi b\Delta b\Delta z$. Thus, the energy loss of the proton due to these electrons is

$$\Delta E(b) = -\left(\frac{1}{4\pi\varepsilon_0}\right)^2 \frac{2e^4 N_e}{m_e b^2 v^2} 2\pi b\Delta b\Delta z \tag{2.18}$$

The total energy loss of the proton can then be obtained by taking the limit $\Delta z \to 0$ and $\Delta b \to 0$ and integrating over the impact parameter b.

$$\frac{dE}{dz} = -\left(\frac{1}{4\pi\varepsilon_0}\right)^2 \frac{4\pi e^4 N_e}{m_e v^2} \int_{b_{\min}}^{b_{\max}} \frac{1}{b}\, db = -\left(\frac{1}{4\pi\varepsilon_0}\right)^2 \frac{4\pi e^4 N_e}{m_e v^2} \ln\left(\frac{b_{\min}}{b_{\max}}\right) \qquad (2.19)$$

We have now derived the main terms and dependencies in the Bethe-Bloch equation (2.3) when we replace v^2 by $c^2\beta^2$, including the main $1/v^2$-dependence of the energy loss on the energy of the proton, and the main material dependence of the stopping power, the proportionality to the electron density N_e.

The factor $[\ln(\Delta E_{\max}/I) - \beta^2]$ in the Bethe-Bloch equation is unfortunately more difficult to derive. In equation (2.19) we have heuristically introduced integration bounds $b_{\min}$ and $b_{\max}$. Qualitatively speaking, the integration bound $b_{\min}$ relates to the maximum energy transfer $\Delta E_{\max}$, and $b_{\max}$ relates to the ionization potential I.

In the limit $b_{\min} \to 0$, the energy loss according to equation (2.19) diverges, which is unphysical. As a first guess, we can instead choose $b_{\min}$ based on the maximum possible energy transfer to an electron. The maximum energy transfer occurs for a head-on collision with conservation of energy and momentum. In the nonrelativistic case, we obtain

$$\Delta E_{\max} = 2 m_e v^2 \qquad (2.20)$$

which is replaced by equation (2.4) in the relativistic case. Together with equation (2.17), this yields

$$b_{\min} = \frac{e^2}{4\pi\varepsilon_0} \frac{1}{m_e v^2} = \frac{2e^2}{4\pi\varepsilon_0} \frac{1}{\Delta E_{\max}} \qquad (2.21)$$

Also in the limit $b_{\max} \to \infty$, the energy loss according to equation (2.17) diverges. Although, the energy transfer to a single electron goes to zero for $b \to \infty$, the number of electrons increases with b. However, at large b, the assumption that the proton scatters with a free electron breaks down. The electrons are bound in atoms and molecules, and consequently the proton cannot transfer an arbitrarily small amount of energy to an electron. A first guess for $b_{\max}$ assumes that the minimum energy transfer is given by the mean ionization potential I. Unfortunately, this choice for $b_{\min}$ and $b_{\max}$ does not quantitatively yield the correct result; however, it provides some intuition why the factor $\ln(\Delta E_{\max}/I)$ appears in the Bethe-Bloch equation.

A more detailed derivation of energy loss of charged particles in matter can be found in the classic textbook by Jackson [1]. In the classical, not quantum mechanical model of an atom, one can calculate the energy transfer of a proton to a harmonically bound electron. This yields a correction term to equation (2.17) which describes the fact the energy transfer to an electron drops to zero faster than $1/b^2$ for large impact parameters.

2.2.4. Range straggling

In sections 2.2.1 to 2.2.3, we considered energy loss of protons in CSDA, which leads to an infinitesimally sharp Bragg peak at the end of range as shown in figure 2.1. In fact, the Bethe-

Bloch equation describes the mean energy loss of protons per unit path length. However, not all protons in a clinical proton beam have exactly the same range. Some protons travel slightly further, others stop slightly before. This effect is called *range straggling*. The effect of range straggling on the depth dose curve can be described by convolving the CSDA depth dose curve obtained from the Bethe-Bloch equation with a Gaussian distribution. As a rule of thumb, the standard deviation of that Gaussian distribution is approximately one percent of the range. Considering a proton beam with 10 cm range, the effect of range straggling corresponds to convolving the CSDA depth dose curve with a Gaussian of 1 mm standard deviation. This is illustrated in figure 2.1 (black line).

The underlying reason for range straggling are statistical fluctuations in the number of collisions of the proton with electrons, i.e. not all protons have exactly the same energy loss per unit distance. This is also the starting point for deriving the expression for range straggling.

Let us revisit equation (2.17) which describes the relation between the impact parameter b and the energy transfer Q to an electron, and equation (2.19) which describes the mean energy loss of a proton per unit distance by integrating over the impact parameter. Using equation (2.17), we can transform the integration over the impact parameter b into an integration over energy levels Q.

$$\frac{dE}{dz} = -\left(\frac{1}{4\pi\varepsilon_0}\right)^2 \frac{4\pi e^4 N_e}{m_e v^2} \int_{b_{\min}}^{b_{\max}} \frac{1}{b}\, db = -\int_{Q_{\max}}^{Q_{\min}} \left(\frac{1}{4\pi\varepsilon_0}\right)^2 \frac{4\pi e^4 N_e}{m_e v^2} \frac{1}{2}\frac{1}{Q}\, dQ \qquad (2.22)$$

On the other hand, we can always express the mean energy loss in general terms as

$$\frac{dE}{dz} = -\int_{Q_{\max}}^{Q_{\min}} n(Q) Q\, dQ \qquad (2.23)$$

when $n(Q)$ is defined as the expected number of collisions with energy transfer Q. Comparing equations (2.22) and (2.23), we can identify that $n(Q)$ is given by

$$n(Q) = \left(\frac{1}{4\pi\varepsilon_0}\right)^2 \frac{4\pi e^4 N_e}{m_e v^2} \frac{1}{Q^2} \qquad (2.24)$$

Collisions with electrons along dz can be considered as a Poisson process. While the proton travels in z-direction, collisions occur at a constant rate and independent of the distance traveled since the last collision. The probability distribution over the number of collisions is then given by a Poisson distribution with mean $n(Q)$. It is a fundamental property of the Poisson distribution that its variance is also equal to $n(Q)$. This allows us to calculate the variance of the energy loss of a proton. The variance of energy loss due to collisions with energy transfer Q is $n(Q)Q^2$ and the total variance is obtained by integration.

$$\frac{d\sigma_E^2}{dz} = -\int_{Q_{\max}}^{Q_{\min}} n(Q) Q^2\, dQ = -\left(\frac{1}{4\pi\varepsilon_0}\right)^2 \frac{4\pi e^4 N_e}{m_e v^2} \frac{1}{2} [Q_{\min} - Q_{\max}] \qquad (2.25)$$

Using the result from equation (2.20) for the maximum energy transfer in a head-on collision, $Q_{\max} = 2m_e v^2$, and $Q_{\min} \ll Q_{\max}$, we obtain

$$\frac{d\sigma_E^2}{dz} = \left(\frac{1}{4\pi\varepsilon_0}\right)^2 4\pi e^4 N_e \tag{2.26}$$

Interestingly, the variance in energy loss is independent of the residual proton energy. It is illustrative to calculate the absolute value of this quantity for water, which yields

$$\sqrt{\frac{d\sigma_E^2}{dz}} \approx 0.3\ [\mathrm{MeV/cm}] \tag{2.27}$$

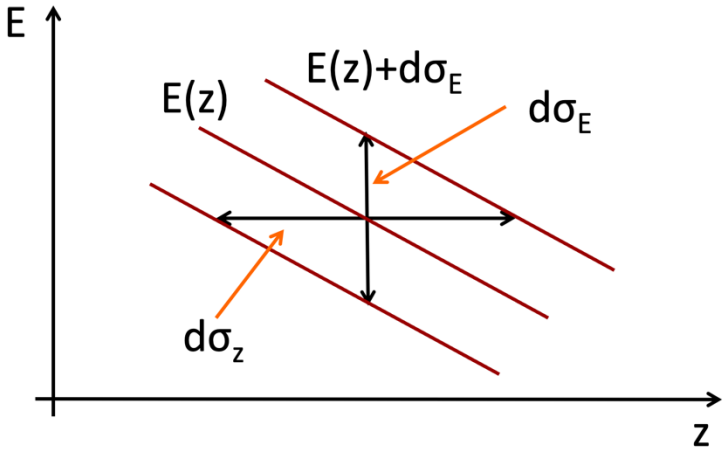

Figure 2.4: Relation of energy and range straggling. When protons travel from depth z to $z + \Delta z$, the variance in the energy spread is increased by $d\sigma_E^2$. This corresponds to a variation in the distance traveled, $d\sigma_z^2$. The ratio of the standard deviations $d\sigma_E/d\sigma_z$ is given by the slope of the function $E(z)$, the residual energy at the current depth.

So far, we have only considered the variance in energy loss and not yet the variance in the range. To obtain the variance of the range, we have to convert variance in the energy loss $d\sigma_E^2$ into variance in distance traveled $d\sigma_z^2$ and then integrate over the entire path of the proton up to the end of range R. Considering the illustration in figure 2.4, we can convince ourselves that

$$d\sigma_E^2 = d\sigma_z^2 \left(\frac{dE}{dz}\right)^2 \tag{2.28}$$

so that the variance of the range is given by

$$\sigma_R^2 = \int_0^R \frac{d\sigma_z^2}{dz} dz = \left(\frac{1}{4\pi\varepsilon_0}\right)^2 4\pi e^4 N_e \int_0^R \left(\frac{dE}{dz}\right)^{-2} dz \tag{2.29}$$

The integral on the right-hand side of (2.29) can be solved numerically using the Bethe-Bloch equation. However, to calculate σ_R^2 in water, we may instead use the power law expression

for dE/dz in equation (2.7), which allows us to obtain an analytical solution. Converting all units to MeV and cm, and inserting the fit parameters $p = 1.77$ and $\alpha = 0.0022$, yields the final result

$$\sqrt{\sigma_R^2} = 0.012\, R^{0.935}\ [\mathrm{cm}] \tag{2.30}$$

2.3. Multiple Coulomb scattering

In section 2.2, we discussed coulomb scattering of protons with electrons, resulting in energy loss of the proton. Due to the large difference between proton and electron mass, we neglected to very good approximation any change in the direction of a proton. We now consider coulomb scattering of protons from nuclei in the medium. As the proton will undergo many such scatters, the effect is widely referred to as *Multiple Coulomb scattering* (MCS). The main consequence of MCS is the broadening of a proton beam with depth. Let us consider an idealized proton pencil beam that is infinitely sharp at the surface of the medium. As a rough rule of thumb, the lateral profile of the beam at the Bragg peak is a Gaussian distribution with a standard deviation that is approximately two percent of the range[6].

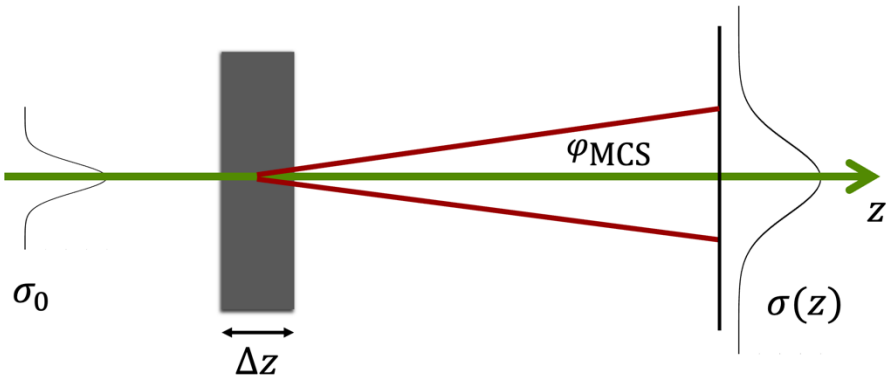

Figure 2.5: Broadening of a Gaussian pencil beam due to multiple coulomb scattering.

To start, we consider the experiment illustrated in figure 2.5. A proton beam with an incident fluence described by a Gaussian distribution of width σ_0 and no divergence hits a scatterer of thickness Δz. The scatterer is thin enough so that the energy is approximately constant, but thick enough so that the protons experience a very large number of scattering events. The net effect is that the beam broadens after the scatterer and the width of the Gaussian fluence distribution increases with distance from the scatterer. Behind the scatterer, protons will be scattered by a random angle φ from the z-axis. The scattering angles follow a Gaussian distribution with zero mean and variance φ_{MCS}^2.

[6] Together with the result for range straggling, this indicates that the Bragg peak of an idealized proton beam (which is infinitely sharp at the surface and has zero initial energy spread and zero divergence) would be sharper in the longitudinal direction than the lateral direction. However, this only describes the theoretical limit. In practice, the initial sigma and energy spread largely impact the sharpness of the Bragg peak.

The goal is to derive φ_{MCS}^2, also referred to as the *mean squared scattering angle* of MCS. In this section, we will derive the so-called Rossi formula, which is often considered the simplest expression to describe MCS. To do so, we will start with the Rutherford cross section that describes a single scatter of a proton from a nucleus. The Rutherford cross section is then used to derive the mean squared scattering angle for MCS.

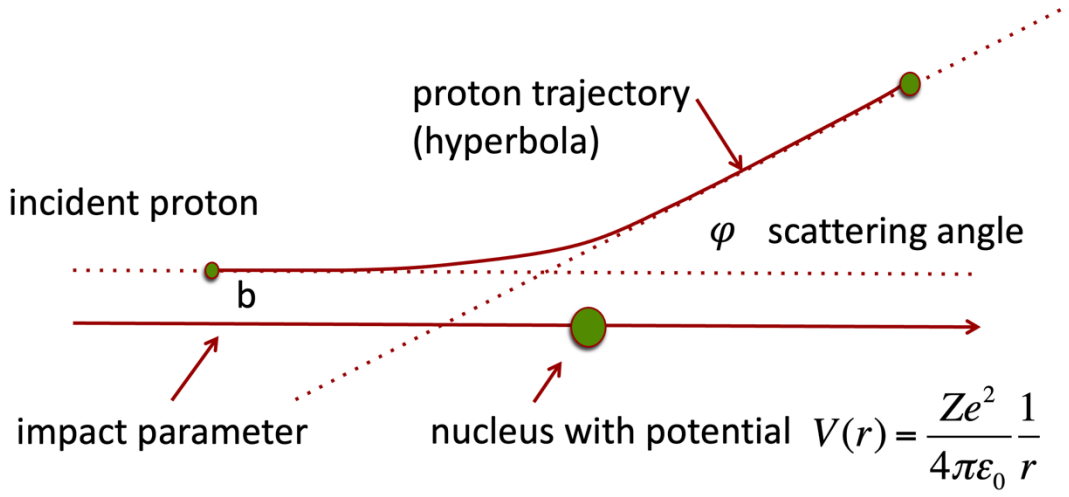

Figure 2.6: Classical model of coulomb scattering of a proton from the coulomb potential of a nucleus.

2.3.1. The Rutherford cross section

Let us consider the classical model of scattering of a proton from the coulomb potential of a nucleus as illustrated in Figure 2.6. Solving the equation of motion yields the trajectory of the proton, which in this case corresponds to a hyperbola. The solution to the equation of motion further yields the relation between the impact parameter b and the scattering angle φ:

$$2\tan\left(\frac{\varphi}{2}\right) = \frac{1}{4\pi\varepsilon_0}\frac{2Ze^2}{m_p v^2}\frac{1}{b} \tag{2.31}$$

where m_p is the rest mass of the proton, Z is the charge of the nucleus that the proton scatters from, and v is the velocity of the incident proton. The scattering angles are small so that we can work with the small angle approximation $\tan(\varphi) \approx \sin(\varphi) \approx \varphi$. Let us consider the protons that are incident at impact parameters between b and $b + db$. These protons hit an area $2\pi b db$ as illustrated in figure 2.7. The fraction of the solid angle that these protons are scattered into is $2\pi \sin\varphi \, d\varphi$. The differential cross section $d\Sigma/d\Omega$ is defined as the ratio

$$\frac{d\Sigma}{d\Omega} = \frac{2\pi b}{2\pi \sin\varphi}\frac{db}{d\varphi} \tag{2.32}$$

Using equation (2.31) to calculate the derivative $db/d\varphi$, we obtain the Rutherford cross section in small angle approximation:

$$\frac{d\Sigma}{d\Omega} = \left(\frac{1}{4\pi\varepsilon_0}\frac{2Ze^2}{m_p v^2}\right)^2 \frac{1}{\varphi^4} \tag{2.33}$$

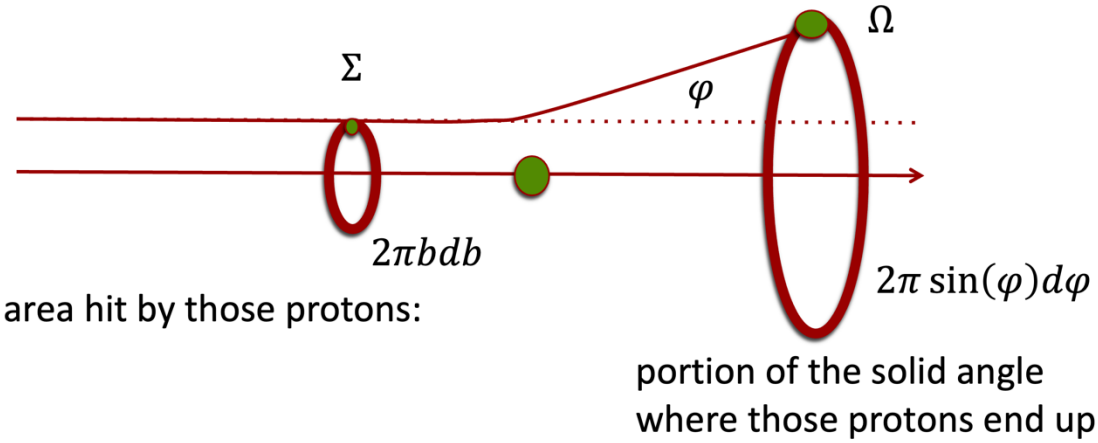

Figure 2.7: Illustration of the Rutherford cross section, defined as the ratio of the area that incident protons hit and the corresponding section of the solid angle that these protons are scattered into.

2.3.2. Mean squared scattering angle for a single collision

The differential cross section divided by the total cross section can be interpreted as the probability distribution over the scattering angle. Therefore, we can calculate the variance $\langle\varphi^2\rangle$ of the scattering angle, i.e. the mean squared scattering angle, by integrating over the solid angle. Since the coulomb potential is symmetric, integration over the azimuth angle yields a factor 2π so that we obtain

$$\langle\varphi^2\rangle = \frac{2\pi}{\Sigma}\int_{\varphi_{\min}}^{\varphi_{\max}} \varphi^2 \left(\frac{1}{4\pi\varepsilon_0}\frac{2Ze^2}{m_p v^2}\right)^2 \frac{1}{\varphi^4}\sin\varphi\, d\varphi \tag{2.34}$$

where Σ is the total cross section. In small angle approximation we obtain

$$\langle\varphi^2\rangle = \frac{2\pi}{\Sigma}\left(\frac{1}{4\pi\varepsilon_0}\frac{2Ze^2}{m_p v^2}\right)^2 \ln\left(\frac{\varphi_{\max}}{\varphi_{\min}}\right) \tag{2.35}$$

2.3.3. The Rossi formula for Multiple coulomb scattering

We now consider protons that traverse a thin sheet of material of thickness Δz. The total scattering angle of a proton is then the result of a very large number of random scattering events that are individually described by the Rutherford cross section. The probability

distribution over the total scattering angle for MCS is Gaussian, even though the differential cross section for an individual collision is described by the $1/\varphi^4$-dependence in equation 2.33. This is a consequence of the central limit theorem. On average, the total scattering angle will be zero. Thus, we are mainly interested in the variance of the scattering angle, i.e. the mean squared scattering angle for MCS. If we assume the scattering events from different nuclei to be statistically independent, this is simply the number of scattering events multiplied by the mean squared scattering angle of a single event. The mean squared scattering angle for MCS is then given by

$$\varphi_{\mathrm{MCS}}^2 = \Delta z\, \Sigma\, N_{\mathrm{Atom}}\, \langle \varphi^2 \rangle \tag{2.36}$$

The number of scattering events is proportional to the thickness of the scatterer Δz, the number of nuclei per unit volume N_{Atom}, and the total cross section for a single coulomb scattering event Σ, which has the dimension of an area. Thus, $\Delta z\, \Sigma\, N_{\mathrm{Atom}}$ is a dimensionless quantity. Inserting 2.35 into 2.36 yields, identifying $\frac{1}{2} m_p v^2$ as the proton energy E, and expressing the nuclei density via

$$N_{Atom} = \rho \frac{N_A}{M_u} \frac{1}{A} \tag{2.37}$$

yields

$$\varphi_{\mathrm{MCS}}^2 = 2\pi \left(\frac{e^2}{4\pi\varepsilon_0} \right)^2 \frac{N_A}{M_u} \ln\left(\frac{\varphi_{\max}}{\varphi_{\min}} \right) \frac{Z^2}{A} \frac{1}{E^2} \Delta z\, \rho \tag{2.38}$$

What remains to be found is an approximation of the integration bounds $\varphi_{\min}$ and $\varphi_{\max}$. For $\varphi_{\min} \to 0$, the mean squared scattering angle diverges. The Rutherford cross section assumes scattering from a Coulomb potential of a nucleus, leading to the result 2.31, where the scattering angle is proportional to the inverse of the impact parameter. Realistically, the scattering angle drops faster to zero than $1/b$ due to the shielding effect of the atomic electrons. Let us assume that we can set $\varphi_{\min}$ such that the corresponding maximum impact parameter $b_{\max}$ is given by the atomic radius, which we express as

$$b_{\max} = 1.4 \left(\frac{4\pi\varepsilon_0 \hbar^2}{m_e e^2} \right) \sqrt[3]{Z} \tag{2.39}$$

We can now summarize the main dependencies in equation 2.38. First, φ_{MCS}^2 is proportional to the thickness of the scatterer Δz. Second, φ_{MCS}^2 is proportional to $1/E^2$ meaning that fast protons are scattered less than protons with a low residual energy. Third, the main material dependence is the proportionality to the mass density ρ and the dependence on the charge of the nucleus which can be summarized as

$$\sim \frac{Z^2}{A} \ln\left(\sqrt[3]{Z} \right) \tag{2.40}$$

It is customary to express the Z-dependence via the *radiation length* L of the scatterer material. The radiation length is the distance at which the energy of high-energy electrons

drops by a factor $1/e$ due to Bremsstrahlung. The radiation length is basically unrelated to coulomb scattering of protons from atomic nuclei but happens to have approximately the same material dependence. The mean squared scattering angle can then be expressed as

$$\varphi_{\mathrm{MCS}} = \frac{K_{\mathrm{Rossi}}}{E}\sqrt{\frac{\Delta z}{L/\rho}} \tag{2.41}$$

Equation 2.41 is called the *Rossi formula* where $K_{\mathrm{Rossi}} \approx 12$ MeV is the Rossi constant. The radiation length of water is approximately 36 cm. For a scatterer of 1 cm thickness and a proton energy of 120 MeV, we obtain $\varphi_{\mathrm{MCS}} \approx 1°$.

2.3.4. Molière theory and further reading

A more accurate and complete theory of MCS is Molière's theory [4], [5]. For a review including experimental evidence and many references but omitting derivations, see Gottschalk et al [6]. For a theoretical derivation in English and a good account of competing theories, see Bethe [7]. The German reader will find Molière's original papers [4], [5] elegant and comprehensive, except that experimental data were sparse at that early date. From Molière's theory, other parameterized formulas for the mean squared scattering angle can be derived, which improve on the Rossi formula (2.41). One of the widely used parameterizations is the Highland formula [8].

2.3.5. Broadening of a proton beam with depth

To conclude the section on MCS, let us consider the width of a proton beam as a function of depth. Let us first consider the situation in figure 2.5. An initially parallel proton beam of width σ_0 hits a scatterer at position $z_1 = 0$ and we are interested in the width of the beam at distance z behind the scatterer. Let us assume that the thickness and material of the scatterer yield a mean squared scattering angle φ_1^2. The sigma of the beam due to MCS in the scatterer is simply $(z - z_1)\tan\varphi_1 \approx (z - z_1)\varphi_1$. The total width of the beam is obtained by adding the variances for the initial width and the broadening due to MCS in quadrature, $\sigma^2(z) = \sigma_0^2 + (z - z_1)^2\varphi_1^2$.

Let us now introduce a second scatterer at position z_2 with mean squared scattering angle φ_2^2 as illustrated in figure 2.8. We can then calculate the total sigma of the beam as $\sigma^2(z) = \sigma_0^2 + (z - z_1)^2\varphi_1^2 + (z - z_2)^2\varphi_2^2$. If we assume that, the patient consists of a stack of scatterers, this can be generalized to

$$\sigma^2(z) = \sigma_0^2 + \int_0^z (z - z')^2 \left[\frac{d\varphi_{\mathrm{MCS}}^2}{dz}\right](z'; E(z'))dz' \tag{2.42}$$

where $[d\varphi_{\mathrm{MCS}}^2/dz](z'; E(z'))$ denotes the *scattering power* of the medium at depth z' for the residual proton energy $E(z')$ at that depth, which may be obtained from the Rossi formula 2.41.

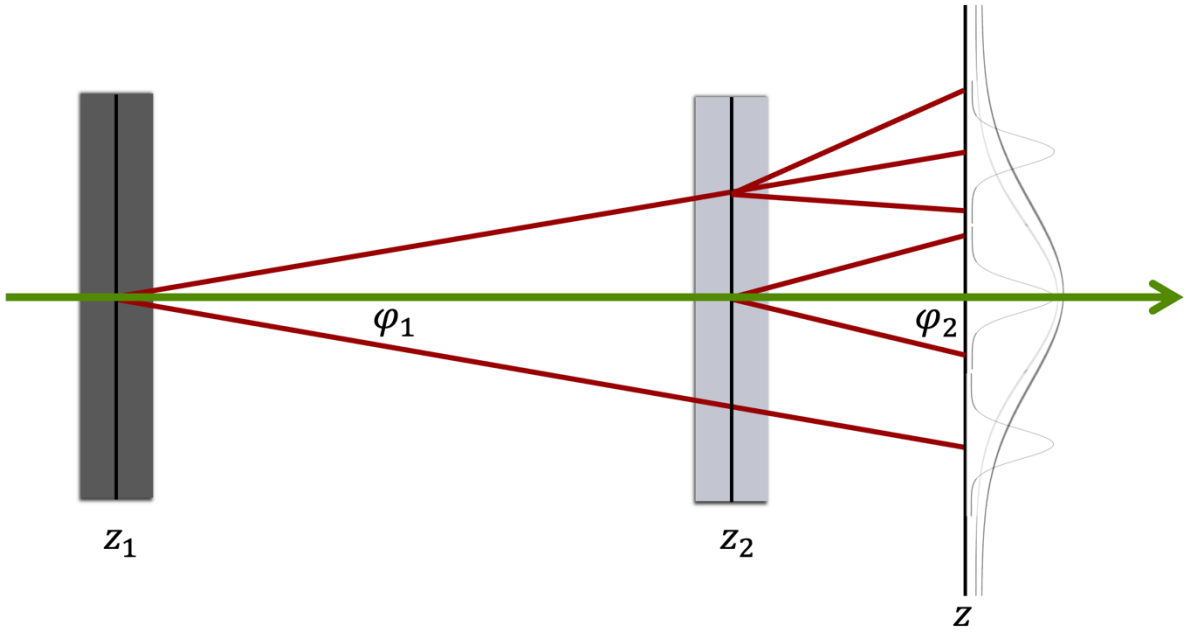

Figure 2.8: Width of a Gaussian proton beam at depth z for the situation that two scatterers at depth z_1 and z_2 are placed in the beam path.

It is interesting to note that the sigma of a proton beam at a given depth depends on the order in which it traverses different materials. Let us consider two proton beams in water with the same initial sigma and the same initial energy. Now, let us introduce a slab of denser bone material of a fixed thickness, which scatters more than water, at different depths. Both beams have the same range. However, a proton beam which first traverses the bone slab has a larger sigma at the Bragg peak compared to a proton beam that first goes through water and traverses the bone slab at a greater depth. This is because the larger scattering angle of the bone slab is weighted with the distance of the Bragg peak from the bone slab.

2.4. Nuclear interactions

In addition to soft electromagnetic interactions discussed in sections 2.2 and 2.3, protons penetrating through matter may undergo nuclear interactions, also referred to as hard scatters [9]. Hard scatters are relatively rare events that occur randomly with a small probability. Considering a 100 MeV proton beam, the number of protons that have a nuclear interaction is in the order of 10%. This contrasts with energy loss discussed in section 2.2, which is the result of myriads of interactions and can be thought of as a mostly deterministic process (except for the small effect of range straggling).

Reactions leading to hard scatters can be categorized in complementary ways. First, they may involve the electromagnetic or the nuclear force. Next, they may be *coherent* (interaction with the nucleus as a whole) or *incoherent* (interaction with a component of the nucleus). Finally, nuclear interactions may be categorized into elastic, inelastic, and nonelastic. For

elastic interactions, the kinetic energy is conserved. The kinetic energy of the incident proton is distributed among the scattered proton and the recoil nuclide, and the recoil nuclide is the same as the target nuclide. In inelastic interactions, the recoil nuclide is the same as the target nuclide, but the kinetic energy is not conserved. The recoil nuclide is left in an excited state. In nonelastic interactions, the recoil nuclide is different from the target nuclide. In the subsections below, we discuss the most important nuclear interactions as examples. The main effects of nuclear interactions on the dose distribution of a proton beam are as follows:

1. *Impact on the integral depth dose curve:* Nuclear interactions lead to a reduction of the primary proton fluence. Consequently, not all protons stop near the Bragg peak. Compared to figure 2.1 where only electromagnetic interactions are considered, this leads to a dose reduction at the Bragg peak, and a corresponding dose increase in the entrance region.
2. *Impact on the lateral beam profile:* Let us consider a Gaussian pencil beam. Nuclear interactions result in larger scattering angles compared to MCS discussed in section 2.3. Some protons are scattered out of the primary proton beam and deposit dose relatively far away from the central axis of the beam. This is commonly referred to as the *nuclear halo* of a proton beam [10].
3. *Relevance for in-vivo range verification and radiation protection:* Inelastic and nonelastic interactions result in neutral secondary particles such as photons and neutrons, which do not have a finite range. Their dose contribution within the radiation field is very small, but they deposit dose outside the radiation field and outside of the patient. Therefore, they play a role for radiation protection. In addition, they are the basis for in-vivo range verification using prompt gamma imaging or positron emission tomography (PET) range verification (chapter 14). The small dose contributions from neutral particles far outside of the radiation field have also been called the *nuclear aura* of a proton beam [10].

For the soft electromagnetic interactions with electrons and atomic nuclei as discussed in sections 2.2 and 2.3, a comprehensive theory exists. The quantitative description of nuclear interactions is in part phenomenological, and the total cross sections and differential cross sections are largely obtained from fits to experimental data[7].

2.4.1. Proton-proton scattering

Hard scattering of protons on free hydrogen $^{1}H(p,p)p$ is elastic, resembling a billiard ball collision between equal masses. The secondaries emerge 90° apart[8] and share the incident energy, the more forward-directed proton being the more energetic. Figure 2.9 illustrates nuclear proton-proton scattering and gives rise to the relation of scattering angle and energy transfer to the recoil proton.

[7] Nuclear Data for Neutron and Proton Radiotherapy and for Radiation Protection, ICRU-Report 63, International Commission on Radiation Units and Measurements, 2000.
[8] In fact, slightly less due to relativistic corrections.

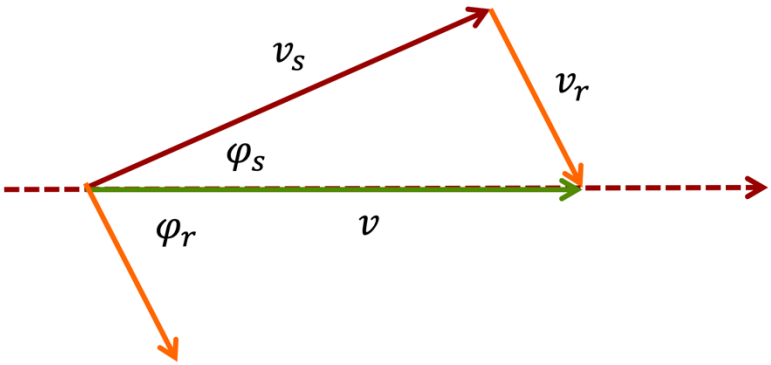

Figure 2.9: Illustration of proton-proton nuclear scattering, representing a billiard ball collision of two equal masses. The relation between scattering angle and energy transfer is obtained from the conservation of energy and momentum.

Let v be the velocity of the incident primary proton, v_s the velocity of the scattered proton, and v_r the velocity of the recoil proton. Since all particles have the same mass, energy conservation (in the nonrelativistic approximation) yields the condition

$$v^2 = v_s^2 + v_r^2 \tag{2.43}$$

Conservation of momentum yields the conditions

$$v_s \cos\varphi_s + v_r \cos\varphi_r = v \tag{2.44}$$

$$v_s \sin\varphi_s + v_r \sin\varphi_r = 0 \tag{2.45}$$

where φ_r and φ_s are the longitudinal scattering angles of the recoil and the scattered proton, respectively. These conditions yield the relation

$$\cos\varphi_s = \frac{v_s}{v} \tag{2.46}$$

for the relation of scattering angle and the velocity of the scattered proton. The differential cross section is such that the probability distribution over the energy of the scattered proton is uniform over the interval $[0, E]$ where E is the energy of the primary proton. The total cross section $\sigma_{pp}(E)$ depends on the energy E of the incident proton. In practice, the total cross sections for nuclear interactions may be obtained by fitting experimental data from databases (see e.g. Fippel et al [11]).

2.4.2. Other nuclear interactions

Another relevant elastic interaction is the scattering of primary protons from ^{16}O nuclei, ^{16}O(p,p)^{16}O, which is conceptually analogous to elastic proton-proton scattering but with different total and differential cross sections. Regarding the interaction's impact on the dose distribution of a proton beam, one relevant aspect is the difference in mass between the

scattered proton and the recoil nucleus. The range of the ^{16}O recoil nucleus is short and the energy transferred to the ^{16}O nucleus is essentially absorbed locally.

Quasi-elastic p-p scattering $^{16}O(p,2p)^{15}N$ is nonelastic. Kinematics resemble scattering on free hydrogen, modified by the binding energy required to extract the target proton, and by the initial momentum of the target proton [12]. Quasi-elastic proton-neutron $^{16}O(p,pn)^{15}O$ scattering is similar, except that one secondary is neutral and travels much farther on average. The resulting ^{15}O is unstable and will undergo β^+ decay with a half-life of about 2 minutes. Annihilation of positron will result in two photons, i.e. two additional neutral particles that, in addition to neutrons, may deposit dose far outside of the radiation field.

2.4.3. Interaction probability and reduction of primary proton fluence

For dose calculation via Monte-Carlo simulations as discussed in the following section, we are interested in the probability that a specific nuclear interaction occurs when the proton travels a small distance dz through the medium. To that end, the total cross section of an interaction, e.g. σ_{pp} for elastic proton-proton scattering can be related to the macroscopic attenuation coefficient μ_{pp}. We can assume that nuclear interactions represent a Poisson process, i.e. the interaction occurs randomly at a constant rate. Generally, the Poisson distribution

$$P(k) = \exp(-\lambda)\frac{\lambda^k}{k!} \tag{2.47}$$

describes the probability that exactly k events happen (here, an event is the nuclear interaction of interest) if the expected number of events is λ. To obtain the probability that the primary proton does not undergo the nuclear interaction, we must evaluate the Poisson distribution for $k = 0$, which yields $\exp(-\lambda)$. The expected number of events can be expressed via the macroscopic attenuation coefficient and the distance traveled, $\lambda = \mu_{pp}dz$. The macroscopic attenuation coefficient in turn is given by the product of the total cross section and the density of scattering centers (here, the density of hydrogen in the medium),

$$\mu_{pp} = \sigma_{pp}\,\rho\,\frac{N_A}{M_u}w_H \tag{2.48}$$

where, as before, N_A is the Avogadro constant, M_u is the molar mass and ρ is the mass density of the medium. w_H denotes the weight proportion of hydrogen in the medium, which is 2/18 for water. The probability for a primary proton to undergo proton-proton scattering over a small distance dz is thus approximately given by

$$P_{pp}(E) = 1 - \exp\left(-\mu_{pp}(E)dz\right) \tag{2.49}$$

Conversely, one can consider the reduction of primary proton fluence $\phi(z)$ in a proton beam with depth z, needed to quantify the impact on nuclear interactions on the depth dose curve in equation 2.2. To that end, all nuclear reactions must be considered. If we denote the total attenuation coefficient by μ (given by the sum of the attenuation coefficients for the individual interactions), we obtain

$$\phi(z) = \phi_0 \exp\left(-\int_0^z \mu(E(z'))dz'\right) \quad (2.50)$$

where the attenuation coefficients depend on proton energy E, and thus indirectly on depth z, even for a homogeneous medium like water. The reduction of primary proton fluence is analogous to the deviation of the exponential depth-dose curve of a photon beam due to (mostly) Compton scattering. The difference is that the exponential attenuation of primary proton fluence only accounts for a small correction of the proton depth dose curve, which is mainly determined by the gradual energy loss of primary protons. In contrast, photons that do not interact via Compton scattering do not deposit any dose at all. The dose is instead deposited by Compton electrons near the interaction point.

2.5. Foundations of proton dose calculation

Starting from the physical interactions of protons in matter discussed in this chapter, Monte Carlo dose calculation algorithms can be seen as the conceptually most straightforward method for dose calculation, which one-to-one translate the basic physics into a dose calculation method. In this section, we will provide an introduction to Monte-Carlo dose calculation, focusing on an understanding of the principles and basic steps of a Monte-Carlo proton transport simulation. We will make simplifying assumptions to focus on the foundations. Therefore, this section is not meant as a state-of-the-art description of Monte-Carlo dose calculation. Later chapters will provide in-depth discussions of Monte-Carlo applications in proton therapy (chapter 14) and dose calculation algorithms (chapter 17). For a comprehensive description of a Monte Carlo dose calculation algorithm for proton therapy see e.g. Fippel et al [11].

2.5.1. A basic Monte-Carlo algorithm for proton dose calculation

Let us consider a 3D volume in which we want to calculate the dose distribution for a given incident radiation field. We assume that the volume is discretized into voxels as illustrated in figure 2.10. We may think of the 3D volume as the computed tomography (CT) of the patient or a phantom. The 3D dose distribution will be represented by the energy deposited in each voxel. We further assume that each voxel is assigned the material properties needed to simulate the interactions of protons.

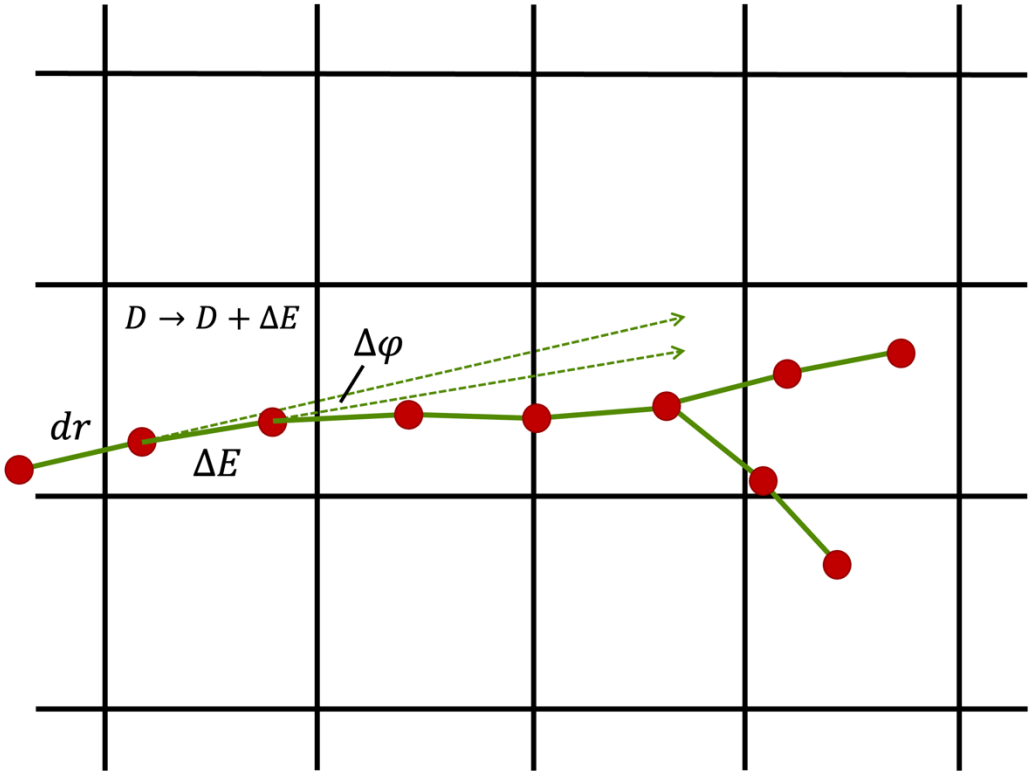

Figure 2.10: Illustration of a Monte Carlo simulation of proton transport through a medium. Red dots represent the discrete positions of the proton; green lines represent the transport of the proton by a distance dr along its current direction. At each step, an energy loss and a change in direction are sampled, and the energy is deposited in the current voxel. On the right, nuclear p-p scattering occurs. Afterward, the transport of both scattered and recoil proton is simulated.

We will simulate the transport of individual protons through the 3D volume. The trajectory of an individual proton is stochastic. The state of a proton at each step of the simulation is described by a 6-dimensional state vector with the following components:

(x, y, z)	position of the proton in 3D space
E	energy of the proton
(φ, θ)	direction of the proton specified by longitudinal and azimuth angle

The initial state of the proton is determined by the incident fluence at the surface of the volume, which depends on the treatment machine and the radiation field. As a simple example, let us assume that a Gaussian pencil beam is centered at $(x = 0, y = 0)$, which is incident along the z-direction and hits the surface of our 3D volume at $z = 0$. Then the position is initialized by randomly sampling (x, y) from a Gaussian distribution with mean $(0,0)$ and a standard deviation corresponding to the width of the pencil beam at the surface. z is set to zero. If we assume that the longitudinal angle is measured against the z-axis and that the proton machine can deliver a perfectly parallel beam with no divergence, the longitudinal angle φ would be initialized to zero. If the beam is slightly divergent but symmetric, we may sample φ from a Gaussian distribution and the azimuth angle θ from a

uniform distribution in the interval $[0,2\pi]$. The proton energy is sampled from a Gaussian distribution centered at a nominal energy E_0 with a small sigma that describes the initial energy spread.

Afterwards, the proton is transported through the 3D volume. To that end, we iteratively perform the following steps, which are in part detailed below and illustrate in figure 2.10:

1. Transport the proton a small step dr along its current direction and update the position (x, y, z) of the proton accordingly.
2. Sample the energy loss ΔE of the proton along the step dr from a Gaussian distribution $\mathcal{N}(\langle\Delta E\rangle, \sigma^2_{\Delta E})$ and subtract ΔE from the current energy of the proton, $E \to E - \Delta E$.
3. Add the energy ΔE to the total energy deposited in the voxel where the proton is located.
4. Sample the change in direction $(\Delta\varphi, \Delta\theta)$ due to MCS from a Gaussian distribution and update the direction of the proton (φ, θ) accordingly.
5. Loop over the relevant nuclear interactions and randomly decide based on the total cross section if the interaction occurs. If a nuclear interaction occurs, simulate the interaction according to the procedure described below.

The simulation of an individual proton is stopped when its energy is zero. If in step 2, the energy loss ΔE is larger than the residual energy, then the residual proton energy is deposited in the current voxel and the simulation is stopped.

Energy loss in step 2:
The energy loss is sampled from a Gaussian distribution. For a sufficiently small step dr, the mean energy loss $\langle\Delta E\rangle$ is obtained from the Bethe-Bloch equation (2.3) and is given by

$$\langle\Delta E\rangle = S(E;\ N_e(x, y, z), I(x, y, z))\ dr \tag{2.51}$$

where $S(E;\ N_e(x, y, z), I(x, y, z))$ is the stopping power for the current proton energy E and the electron density and ionization potential at the current position (x, y, z). The variance of the energy loss $\sigma^2_{\Delta E}$ due to energy straggling is given by equation (2.26),

$$\sigma^2_{\Delta E} = \left(\frac{1}{4\pi\varepsilon_0}\right)^2 4\pi e^4 N_e(x, y, z)\ dr \tag{2.52}$$

MCS in step 4:
The change in direction $(\Delta\varphi, \Delta\theta)$ is sampled from a 2D Gaussian distribution with zero mean and a standard deviation obtained from the Rossi formula in equation (2.41), given the current proton energy E and the radiation length $L(x, y, z)$ of the current voxel.

Nuclear interactions in step 5:
The probability for a nuclear interaction is quite small. For a step size dr of 1 mm, the probability of a nuclear interaction is in the order of 0.1%. The steps needed to simulate a nuclear interaction depend on the specific interaction. We use elastic p-p scattering as an example.

5. Calculate the probability $P_{pp}(E)$ of the interaction along the step dr from equation (2.49) from the total cross section of the interaction, given the current proton energy E. Sample a uniformly distributed random number q in the interval $[0,1]$. If $q > P_{pp}(E)$ continue; if $q < P_{pp}(E)$, simulate the interaction according to the following steps:
    a. Sample the energy of the scattered proton based on the differential cross section of the interaction. For elastic p-p-scattering, this amounts to sampling a uniformly distributed random number E_s in the interval $[0, E]$ and assign the scattered proton the energy E_s.
    b. Create the recoil proton at the position (x, y, z), which afterwards is simulated just like a primary proton. Assign the recoil proton the energy $E - E_s$.
    c. Calculate the longitudinal scattering angle $\Delta\varphi_s$ corresponding to the energy E_s. Sample an azimuth angle $\Delta\theta_s$ from a uniform distribution and update the direction of the scattered proton (φ, θ) accordingly. Set the direction of the recoil proton accordingly.

Other elastic interactions such as elastic scattering from ^{16}O are simulated in an analogous manner, except that the appropriate total and differential cross sections must be used.

Transport of secondary particles:
In the basic algorithm described here, we consider only the transport of protons and assume that secondary particles other than protons deposit their dose locally. This is mostly correct for proton therapy dose calculation where a typical voxel size is in the order of 1 mm. Recoil nuclides heavier than protons created in nuclear interactions have short range, and their energy can to good approximation be deposited locally. Photons and neutrons do not deposit their energy locally. Their transport can be simulated using general-purpose Monte Carlo codes (chapter 11); however, their dose contribution within the treatment field is small. Electrons deposit their dose mostly locally; however, the electrons with the highest energy, so-called δ-electrons, may have a range that exceeds the typical size of a voxel. Monte-Carlo dose calculation may be improved by simulating the transport of these high-energy electrons separately (chapter 11).

2.5.2. Illustration of Monte-Carlo dose calculation

Let us illustrate Monte-Carlo dose calculation using the basic algorithm described above. We consider a parallel Gaussian beam of 100 MeV protons incident along the z-direction with a sigma of 5 mm at the patient surface. For simplicity and the sake of illustration, we consider a 2-dimensional world where all protons are confined to the (x, z)-plane. The second lateral dimension y is ignored by sampling only a longitudinal scattering angle in the (x, z)-plane but no azimuth angle. Also, from all nuclear interactions, we consider only elastic p-p scattering using the cross sections described in Fippel et al [11].

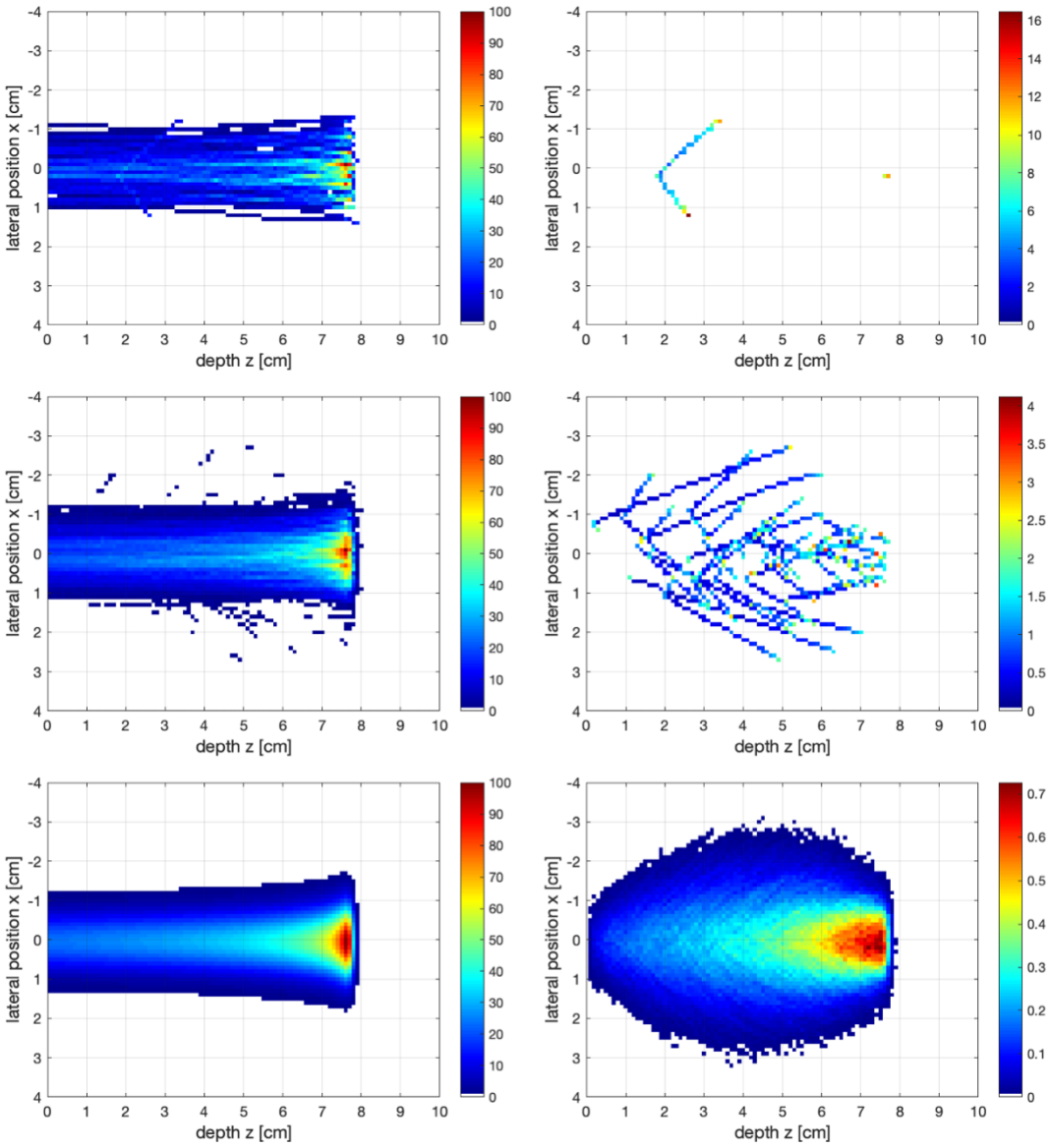

Figure 2.11: Illustration of a two-dimensional Monte Carlo dose calculation in water for a 100 MeV Gaussian proton beam of 5 mm width at the surface, following the algorithm in section 2.5.1. From all nuclear interactions, only elastic proton-proton scattering is simulated. Left column: Total dose deposited (in percent of the maximum value); Right column: Dose contribution of secondary protons resulting from elastic proton-proton scattering (in percent of the maximum total dose). Different numbers of primary protons are simulated. Top row: 100 protons, illustrating individual trajectories or events: Middle row: 1000 protons; Bottom row: 1000000 protons, showing the smooth dose distribution of a proton pencil beam.

Let us first consider the dose distribution in water. For the calculation of the mean energy loss via the Bethe-Bloch equation, we assume a mean ionization potential of 75 eV; to calculate the mean squared scattering angle according to the Rossi formula, we assume 36 cm as the radiation length of water. Figure 2.11 (bottom left) shows the dose distribution resulting from

a simulation of one million primary protons. The figure shows the familiar Bragg peak and the correct range of 7.8 cm. Figure 2.11 (bottom right) shows the part of the nuclear halo that originates from secondary protons created through nuclear p-p scattering of a primary proton. To that end, the scattered and recoil protons have been flagged and their dose contribution has been scored separately from the dose deposition of primary protons. The figure illustrates the broader width of the halo compared to the width of the primary beam, which broadens only moderately with depth due to MCS. To parameterize the dose distribution of a proton beam, one often uses the sum of two Gaussian distributions for the lateral distribution, one for the primary protons and one for the nuclear halo (chapter 14).

Figure 2.11 (top row) shows the simulation of 100 primary protons to illustrate individual random proton trajectories. In this example, two protons have a nuclear interaction. One event occurs in the entrance region of the beam, illustrating the possibility of large scattering angles in nuclear interactions, compared to the relatively small deflections of primary protons due to MCS. The second nuclear interaction occurs close to the Bragg peak so that the resulting secondary protons have short residual range.

As an illustration of dose calculation in a heterogeneous medium, we consider the phantom geometry in figure 2.12 where we insert an inhomogeneity between depth $z = 1$ and $z = 2$. For $x < 0$ we assume a denser material with mass density $\rho = 2$ resembling dense bone; for $x > 0$ we assume a less dense material with mass density $\rho = 1/3$ resembling lung tissue. For simplicity, we assume that the relevant material properties - stopping power, radiation length, and the probability of nuclear p-p-scattering - simply scale with mass density. Protons that traverse the lung-like material penetrate further into the phantom and stop approximately 2/3 of a cm deeper in the phantom. This is because the energy loss in 1 cm of lung-like material corresponds to 1/3 cm of water. Protons that traverse the bone-like material penetrate less deep into the phantom and stop approximately 1 cm closer to the surface. This is because the energy loss in 1 cm of bone-like material corresponds to 2 cm of water. The Bragg peak is thus degraded due to the lateral tissue heterogeneities. Due to MCS, protons do not travel along a straight path. A proton may go through the lung slab and therefore stop deep in the phantom, but slightly change direction after the inhomogeneity to end up behind the bone slab. Therefore, the degraded Bragg peak still shows a smooth dose distribution instead of featuring a sharp dose falloff at $x = 0$.

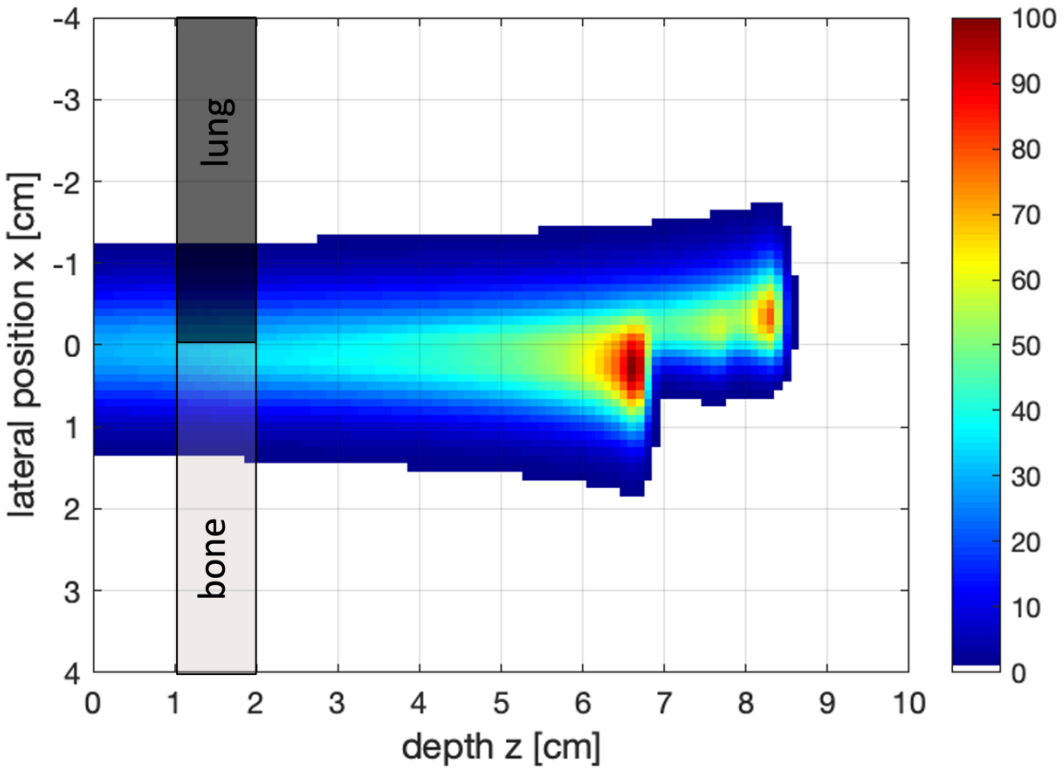

Figure 2.12: Monte Carlo dose calculation in a heterogeneous phantom for a 100 MeV Gaussian proton beam of 5 mm width at the surface, simulating 1 million primary protons. Protons pass through a heterogeneity between $z = 1$ and $z = 2$, consisting of bone-like material for $x < 0$ and lunge-like material for $x > 0$. The remaining phantom is water.

2.5.3. Deterministic dose calculation based on transport equations

In a Monte-Carlo simulation of proton transport, the state of a proton can be described by a 6-dimensional vector. If we simulate enough protons, this gives rise to a distribution function

$$f(x, y, z, E, \varphi, \theta) \tag{2.53}$$

which describes how many protons we have at position (x, y, z) that go in direction (φ, θ) with energy E. f may also be called the phase space density. A Monte-Carlo simulation can be interpreted as a sampling method that draws random samples from the distribution f.

Instead of using a sampling method, one may attempt to calculate f via deterministic methods [13], [14], [15]. To that end, a Boltzmann transport equation can be formulated that describes proton transport. The transport equation represents a partial differential equation (PDE) for the phase space density f, and the boundary conditions are specified by the incident radiation field. Numerical solution of the PDE in principle yields f, which is however a computationally challenging task.

From the distribution function f, we can calculate the energy fluence vector field $\vec{\psi}(x,y,z)$, which describes how much energy is transported by protons at position (x,y,z) in each direction. The dose deposited at position (x,y,z) can formally be defined as the divergence of the energy fluence vector field:

$$D(x,y,z) = -\frac{1}{\rho}\operatorname{div}\vec{\psi}(x,y,z) = -\frac{1}{\rho}\left[\frac{\partial\psi_x}{\partial x} + \frac{\partial\psi_y}{\partial y} + \frac{\partial\psi_z}{\partial z}\right] \tag{2.54}$$

This is the 3-dimensional generalization of our simple 1-dimensional model of the proton depth dose curve in equation (2.1) presented in the very beginning of this chapter. Equation (2.54) has an intuitive interpretation if we recall the Gauss theorem from vector calculus.

$$\iiint_V \operatorname{div}\vec{\psi}(x,y,z)\,dV = \oiint_S \left(\vec{\psi}\cdot\vec{n}\right)dS \tag{2.55}$$

The Gauss theorem in our situation states that the integral of the divergence of the energy fluence vector field over a volume V equals the integral of the energy flow through a closed surface S around volume V, which in turn is the total energy deposited in volume V.

References

[1] J. D. Jackson, *Classical Electrodynamics*. John Wiley & Sons, 1998.

[2] R. D. Evans, *The Atomic Nucleus*. McGraw-Hill, 1955.

[3] T. Bortfeld and W. Schlegel, "An analytical approximation of depth-dose distributions for therapeutic proton beams," *Phys Med Biol*, vol. 41, no. 8, pp. 1331–1339, Aug. 1996, doi: 10.1088/0031-9155/41/8/006.

[4] G. Moliere, "Theorie der Streuung schneller geladener Teilchen I. Einzelstreuung am abgeschirmten Coulomb-Feld," *Zeitschrift für Naturforschung A*, vol. 2, no. 3, pp. 133–145, Mar. 1947, doi: 10.1515/zna-1947-0302.

[5] G. Molière, "Theorie der Streuung schneller geladener Teilchen II. Mehrfach- und Vielfachstreuung," *Zeitschrift Naturforschung Teil A*, vol. 3, pp. 78–97, Feb. 1948, doi: 10.1515/zna-1948-0203.

[6] B. Gottschalk, A. M. Koehler, R. J. Schneider, J. M. Sisterson, and M. S. Wagner, "Multiple Coulomb scattering of 160 MeV protons," *Nuclear Instruments and Methods in Physics Research Section B: Beam Interactions with Materials and Atoms*, vol. 74, no. 4, pp. 467–490, Jun. 1993, doi: 10.1016/0168-583X(93)95944-Z.

[7] H. A. Bethe, "Moli\`ere's Theory of Multiple Scattering," *Phys. Rev.*, vol. 89, no. 6, pp. 1256–1266, Mar. 1953, doi: 10.1103/PhysRev.89.1256.

[8] V. L. Highland, "Some practical remarks on multiple scattering," *Nuclear Instruments and Methods*, vol. 129, no. 2, pp. 497–499, Nov. 1975, doi: 10.1016/0029-554X(75)90743-0.

[9] H. Paganetti, "Nuclear interactions in proton therapy: dose and relative biological effect distributions originating from primary and secondary particles," *Phys Med Biol*, vol. 47, no. 5, pp. 747–764, Mar. 2002, doi: 10.1088/0031-9155/47/5/305.

[10] B. Gottschalk, E. W. Cascio, J. Daartz, and M. S. Wagner, "On the nuclear halo of a proton pencil beam stopping in water," *Phys Med Biol*, vol. 60, no. 14, pp. 5627–5654, Jul. 2015, doi: 10.1088/0031-9155/60/14/5627.

[11] M. Fippel and M. Soukup, "A Monte Carlo dose calculation algorithm for proton therapy," *Med Phys*, vol. 31, no. 8, pp. 2263–2273, Aug. 2004, doi: 10.1118/1.1769631.

[12] H. Tyrén, S. Kullander, O. Sundberg, R. Ramachandran, P. Isacsson, and T. Berggren, "Quasi-free proton-proton scattering in light nuclei at 460 MeV," *Nuclear Physics*, vol. 79, no. 2, pp. 321–373, Apr. 1966, doi: 10.1016/0029-5582(66)90149-0.

[13] J. L. Bedford, "A discrete ordinates Boltzmann solver for application to inverse planning of photons and protons," *Phys Med Biol*, vol. 68, no. 18, p. 185019, Sep. 2023, doi: 10.1088/1361-6560/acf4de.

[14] J. L. Bedford, "Calculation of absorbed dose in radiotherapy by solution of the linear Boltzmann transport equations," *Phys Med Biol*, vol. 64, no. 2, p. 02TR01, Jan. 2019, doi: 10.1088/1361-6560/aaf0e2.

[15] G. A. Sandison and A. V. Chvetsov, "Proton loss model for therapeutic beam dose calculations," *Med Phys*, vol. 27, no. 9, pp. 2133–2145, Sep. 2000, doi: 10.1118/1.1288681.